JOM
https://doi.org/10.1007/s11837-023-05707-8

THE INCORPORATION OF SECONDARY AND RECYCLED MATERIALS IN A PRIMARY SMELTING FLOWSHEET

Energy Consumption and Greenhouse Gas Emissions of High-Carbon Ferrochrome Production

WENJING WEI,[1,2,3] PETER B. SAMUELSSON,[1] PÄR G. JÖNSSON,[1] RUTGER GYLLENRAM,[1,2] and BJÖRN GLASER[1]

1.—Department of Materials Science and Engineering, KTH, Royal Institute of Technology, Stockholm, Sweden. 2.—Kobolde & Partners AB, Ringvägen 100, 118 60 Stockholm, Sweden. 3.—e-mail: wenjingw@kth.se

This work presents a process model developed based on mass and energy conservation to assess high carbon ferrochrome production from cradle to gate through four supply routes: (1) a conventional submerged arc furnace (SAF), (2) a closed submerged arc furnace with preheating (CSAF+PH), (3) a closed submerged arc furnace with 60% prereduction (CSAF+PR60%) and (4) a direct-current arc furnace (DCAF). The energy requirements are between 40 and 59 GJ/t FeCr (74–111 GJ/t Cr), and the greenhouse gas (GHG) emissions range between 1.8 and 5.5 tCO_2-eq/t FeCr (3.3–10.3 tCO_2-eq/t Cr). The upgrading of coal-powered SAF process to a closed furnace CSAF+PH and CSAF+PR60% contributes to an emission reduction of 23% and 18%, respectively. Moreover, the use of hydro-powered electricity leads to a further emission reduction of 68% and 47%, respectively. For CSAF+PR process, the GHG emissions can be reduced by 14% when increasing the pre-reduction ratio from 30% to 80% and decreased by 10% when charging hotter feed from 100 °C to 1000 °C. The proposed process model is feasible in generating site-specific inventory data and allowing for parameter studies as well as supporting companies to improve the transparency of the environmental performance in the FeCr value chain.

Abbreviations

AOD	Argon oxygen decarburization
DC	Direct current
DCAF	Direct-current arc furnace
CSAF+PH	Closed submerged arc furnace with preheating
CSAF+PR60%	Closed submerged arc furnace with 60% pre-reduction
EF	Emission factor
GHG	Greenhouse gas
GWP	Global warming potential
HC FeCr	High carbon ferrochrome
LCA	Life cycle analysis
LC FeCr	Low carbon ferrochrome
PEF	Primary energy factor
SAF	Submerged arc furnace
VOD	Vacuum oxygen decarburization

INTRODUCTION

Chromium is an indispensable alloy element in stainless steelmaking, with chromium oxide being the major compound resisting corrosion by forming a passive film on the steel surface.[1] In the 300 series stainless steel, the content of chromium can reach up to 25%. The demand for low-carbon ferrochrome (LC FeCr) has decreased dramatically with the development of argon oxygen decarburization (AOD) and vacuum-oxygen-decarburization (VOD) technologies. This enables the use of inexpensive high-carbon ferrochrome (HC FeCr) in stainless steelmaking. HC FeCr is available in two typical specifications: ordinary high carbon ferrochrome and so-called charge chrome, varied in the alloy content. Ordinary HC FeCr typically contains 60–70% Cr and 4–6%C, which is commonly found in FeCr processed from Kazakhstan ore that has high Cr/Fe ratios (~3.8).[2,3] Charge chrome has a

(Received September 3, 2022; accepted January 16, 2023)

relatively lower chromium content, namely between 50% and 55%,[3] which can be found in FeCr from South African ores and has a low Cr/Fe ratio of 1.3.[2]

Increased raw material and energy prices together with demands from the stainless steel producers to abate the emission of greenhouse gases (GHG) impose challenges on the FeCr producers. The production of 1 tonne stainless steel emits 2.93 tonnes of CO_2 on average, where raw materials account for 70% and Cr accounts for 30% of the total greenhouse gas emissions.[4] Thus, it is necessary to perform investigations on raw materials to improve the environmental profile of stainless steel.

Life cycle analysis (LCA) is a typical tool to assess the environmental impacts such as global warming potential (GWP) by accounting for the resource consumption (material and energy) through all the stages of the life cycle of a product, process or service. It is used for decision making, forming public policy and improving environmental performance. However, the LCA methodology also has some limitations. First, the required data in an assessment include the material and energy used to produce a specific product as well as material and energy losses during the production process. This information is normally reported at an aggregated industry level since this type of information is considered confidential by the companies. If the LCA studies are carried out based on aggregated data, either aggregated company data or aggregated product data, this represents an average level for a company. Such information becomes less useful for a customer wanting to improve the sustainability performance of a supply chain. Therefore, shortage of site- and product-specific information brings difficulties for downstream steel producers to assess and report their upstream GHG emissions, often reported as scope 3 data in Greenhouse Gas Protocol.[5] Second, the data collection process can be both time and resource consuming, depending on the depth and the assumptions used in the study. For the LCA expert who is not from the expertise domain, it becomes more difficult to judge the data selection. Thus, there is an obvious risk of bias of any assessment carried out by an industry or a representative, especially when the assessment and conclusions are supporting an economic interest.[6] Moreover, the concept of considering each production stage as a 'black box', only using inputs and outputs, neglects the correlation between operation parameters and consumables. It doesn't provide a transparency and understanding of the production process behind a product, limiting the product optimization potential in design and operation.[7,8]

In the current work, a process model based on mass and energy conservation is proposed to investigate the primary energy use and emission impacts of greenhouse gases of producing high-carbon ferrochrome from cradle to gate. This process modelling approach, based on the law of conservation of mass and energy, has been widely applied in performance analysis of different pyrometallurgical processes, such as the production of lime,[9] steel,[10] nickel[11,12] and silicon.[13] The developed process model is based on the public data available in open literature, which is subject to review by all interested parties and can be less biased. The methodology is intended to be used for supporting companies to improve the transparency of the environmental performance in the FeCr value chain.

PRODUCTION ROUTES OF HC FECR

In 2020, global ferrochrome production was 12.7 million tonnes in which China, South Africa and Kazakhstan rank as the top three producers.[14] Chromite ($FeCr_2O_4$) ore is today the only economical chromium resource that contains about 45%Cr_2O_3. It is extracted by either open-pit or underground method.[15] HC FeCr is typically produced by a carbothermic reduction of chromite ore in either a submerged arc furnace (SAF) or a direct current (DC) arc furnace. The carbides (e.g., Cr_7C3, Cr_3C_2) form prior to the metallic Cr during smelting process because of the low Gibbs free energy for the formation of carbides under most smelting temperature ranges;[15] see typical chemical reactions in Eqs. 1–14.[16,17] The three-phase SAF smelting has traditionally been the dominating production technology for ferrochrome. There are three types, namely: (1) an open type, (2), a semi-closed (3) and a closed type. The use of closed type furnaces makes it possible to utilize off-gas, which is rich in CO, for process heating. The submerged arc furnace buries the three electrodes in the burden material, while the DC arc furnace is operated with an open slag bath and applies a single hollow graphite electrode as the cathode.

Sintering:

$$H_2O(l) = H_2O(g) \tag{1}$$

$$4FeO(s) + O_2(g) = 2Fe_2O_3(s) \tag{2}$$

Prereduction:

$$Fe_2O_3(s) + CO(g) = 2FeO(s) + CO_2(g) \tag{3}$$

$$FeO(s) + C(s) = Fe(s) + CO(g) \tag{4}$$

$$Cr_2O_3(s) + 3C(s) = 2Cr(s) + 3CO(g) \tag{5}$$

$$Fe_2O_3(s) + CO(g) = 2FeO(s) + CO_2(g) \tag{6}$$

Smelting:

$$FeO(s) + C(s) = Fe(l) + CO(g) \tag{7}$$

$$7Cr_2O_3(s) + 27C(s) = 2Cr_7C_3(l) + 21CO(g) \tag{8}$$

$$6Cr_2O_3(s) + 26C(s) = 4Cr_3C_2(l) + 18CO(g) \tag{9}$$

$$SiO_2(s) + 2C(s) = Si(l) + 2CO(g) \quad (10)$$

$$C(s) + O_2(g) = CO_2(g) \quad (11)$$

$$C(s) + CO_2(g) = 2CO(g) \quad (12)$$

$$H_2O(l) + C(s) = CO(g) + H_2(g) \quad (13)$$

$$CaCO_3(s) = CO_2(g) + CaO(s) \quad (14)$$

In summary, there are currently four common process technologies or production routes that are commercially used in producing HC FeCr, listed below. A comparison of the four production routes is described in Table S-1 (refer to online supplementary material).

- Conventional open/semi-closed submerged arc furnace **(SAF)**
- Closed submerged arc furnace with preheating **(CSAF+PH)**
- Closed submerged arc furnace with prereduciton **(CSAF+PR)**
- Direct-current arc furnace **(DCAF)**.

Conventional Open/Semi-Closed Submerged Arc Furnace (SAF)

Conventional submerged arc furnaces are still widely used in HC FeCr production.[18] Ores are charged together with reductants and fluxes, and the output of SAF is off-gas, slag and alloy. This technology is characterized by simple operation, a low capital cost and flexibility with respect to the feed. Meanwhile, the drawbacks are, for instance, a lower thermal efficiency and metal recovery.[3,19] A large amount of off-gas generation and higher heat losses through the furnace bed and sidewalls result in lower thermal efficiencies in this operation. Furthermore, there are potential losses of the unreduced fine materials while de-slagging.

Closed Submerged Arc Furnace with Preheating (CSAF+PH)

The closed submerged arc furnace is generally of a larger scale compared to an open SAF, which brings the need to form a permeable raw material bed for the process gas. Thus, it requires an optimal ore agglomeration to facilitate stable operation. Raw materials such as ore and coke are milled, mixed and pelletized. Green pellets of some 12 mm in diameter are delivered to a sintering plant using, for example, a steel conveyor belt. Other than the energy from the blended coke combustion, the pellets are dried/preheated and sintered by the recycled hot circulating cooling gas to sustain the sintering temperature at 1400°C.[3,20] During the sintering process, the free/bonded water is removed from the feed and Fe^{2+} is oxidized into Fe^{3+}. The sintered pellets are then discharged from the belt at around 100°C after air cooling and then transported to the smelter.[20,21] The feed mixture consists of sintered pellets, lumpy ore, coke and quartzite, which are first preheated to 600–700°C with the hot and combusted off-gas. The preheater can be a shaft kiln located above the submerged arc furnace. The feed's moisture is removed and then materials leave the preheater at about 500 °C.[3] The electricity input in a closed SAF furnace is significantly decreased after preheating. Due to a good sealing system, the closed SAF furnace forms a CO-rich off-gas (75–90% CO), which mainly depends on the feeding ratio between the pellets and lumpy ore.[22] A higher lumpy ore content in the feed mixture generates a higher volume of H_2O and CO_2 and a smaller volume of CO. These gases are good secondary fuel sources that are practically utilized in sintering, preheating and other processes.[22]

Closed Submerged Arc Furnace with Prereduction (CSAF+PR)

Like when using the preheating route, the ore concentrate, anthracite and bentonite are first dried and then milled before being pelletized using this prereduction process technology. A pellet diameter size of some 10–30 mm is desired to avoid over-roasting, which can result in a low metallization degree.[23] The prereduction process takes place in a long travelling grate. The green pellets are dried and partially reduced at about 1300 °C. Normally, a higher reduction degree of pellets leads to a lower electricity consumption in the smelter but also a lower productivity of the system (CSAF+PR).[23] The energy in the rotary kiln is supplied at the end of the kiln by the combustion of recycled off-gas and coal-powered combustion with oxygen or air. Hot pre-reduced pellets are discharged into the submerged arc furnace together with coke and flux to enable the smelting process. The off-gas is possible to collect and use for preheating in the production process.

Direct-Current Arc Furnace (DCAF)

In the submerged arc furnace, the arc is buried in the slag and the charge.[24] It normally has a requirement of using a permeable burden material, a proper slag's liquidus temperature and electrical resistivity.[25] In the DC arc furnace is operated using open bath smelting, the arc burns freely in the furnace. The furnace is equipped with either a single solid graphite electrode or a hollow electrode. DC arc smelting is independent of the slag's chemistry. This provides freedom with respect to the slag composition and process temperature. In addition, the lower demand of feed quality reduces the capital cost.[3,26] Compared to the submerged arc furnace, the DC arc furnace can maintain the furnace's voltage and temperature at a constant and high level because it is operated using a longer arc between electrode and melt.[3,27] However, some limitations still exist in this operation. First, it requires higher power consumption because of the heat losses through the furnace roof and walls by radiation from the bath and arc. Second, the direct contact of bath and furnace linings results in a shorter lifetime of the refractories.

METHODOLOGY

System Boundary

The process model based on energy and mass conservation consists of the following steps to assess energy consumption and greenhouse gas emission from cradle to gate, given in Fig. 1a:

- Mining and ore processing (beneficiation)
- Pre-processing (pelletizing/prereduction/sintering)
- Smelting (preheating)

The steps in the pre-processing part of the process may vary depending on the smelting technology employed. The functional unit is 1 tonne of ferrochrome alloy. The inventory dataset was established through the calculations using the process model, which is based on a mass and energy conservation. The established inventories were applied to calculate the greenhouse gas emissions. The GHG emissions for using cooling water, explosives, compressed air and transport of raw materials are considered to have a low impact and are excluded in this study.

Description of Process Model Based on Mass and Energy Balance

A process model based on the laws of the conservation of mass and energy has been developed in this work, which states that the total mass/energy entering a defined system is equal to the total mass/energy leaving the system. The typical input or consumptions in a process consist of chromium-containing materials (ore/concentrate/pellets/prereduced pellets/sinter), oxidation gases (oxygen/air), reductants (coal/coke/anthracite), slag formers (lime/silica), fossil fuels and recycled off-gas. The typical outputs from the process are intermediate chromium product, slag, off-gas and dust. In the energy balance, the ingoing energies include electricity, fuel, enthalpy of charged materials and exothermic reaction heats. Furthermore, outgoing energies are also present as thermal heat stored in the processed product, slag, flue gas and furnace heat loss as well as endothermic reaction heat.

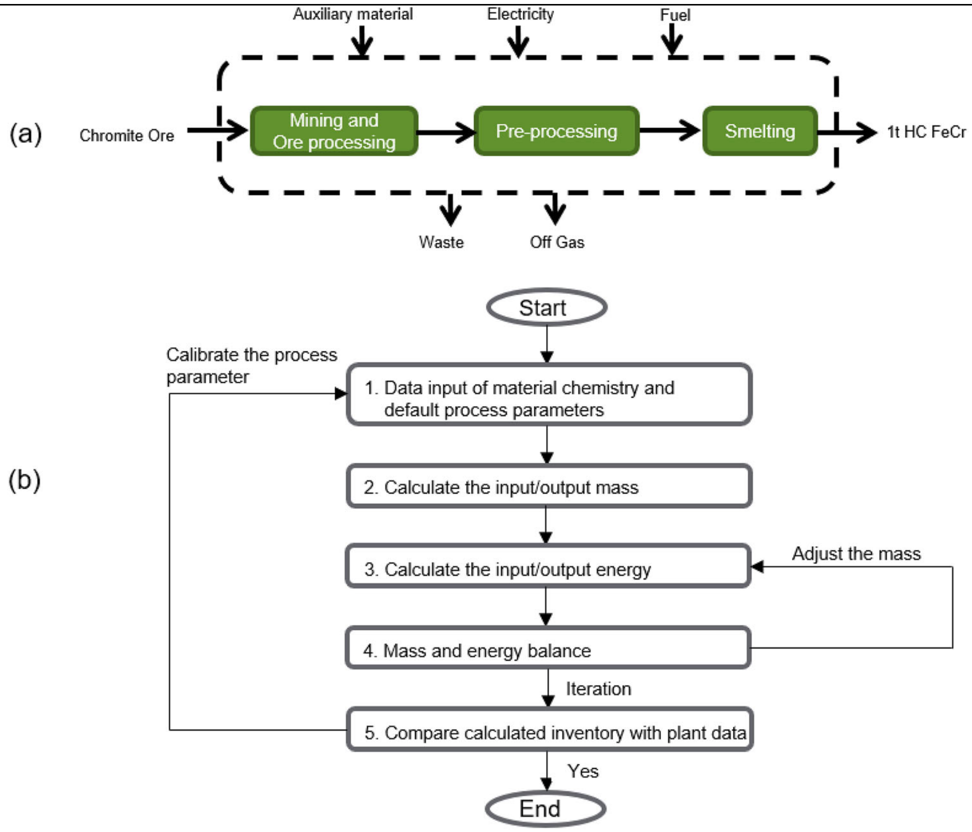

Fig. 1. (a) System boundary of producing 1 tonne HC FeCr from cradle to gate. (b) Calculation sequence of the static process model based on mass and energy balances.

The following calculation sequence was applied for the mass and energy balance in the process model, illustrated in Fig. 1b:

1. Use the chemistry of chromite and auxiliary materials as the initial data. Set default value of some modelling parameters, for instance, the metal recovery rate, slag basicity, heat loss ratio, chemistry specification of the output source, operation, and discharge temperature. These values can be collected from published sources such as articles, reports, company websites, etc.
2. Calculate the input and output mass based on reactions and metal distribution factors.
3. Calculate the input and output enthalpy. Adjust the fuel and energy requirement through iterations.
4. Fulfil the conditions of both the mass and energy balances.
5. Obtain the inventory data of this process. Compare the calculated inventory with published plant data if available. Calibrate the process parameters.
6. If the process is divided into multi-steps, use the output of intermediate products as input in the subsequent process steps.
7. Repeat step 1–5 until the final chromium alloy is produced.

The following assumptions are made to simplify the creation of the mathematical model:

- The modelling system is in a steady state, which means that the balance is independent of time. The reference temperature is 298.15 K.
- The entered gases, if not stated, are ideal and are calculated based on stoichiometry rather than an excess amount used in the reduction condition.
- Fuel combustion includes carbon oxidation for energy balance. When accounting for the total primary energy and GHG emissions, the energy and emission factors are taken from the literature (see Table I). In the mass balance module, a complete fuel combustion condition was assumed to calculate the amount of oxidation gas and flue gas.
- Modelling of sintering (Case 2) includes four zones on the steel belt: drying, sintering, primary cooling and secondary cooling. The drying zone utilizes the off-gas heat from the secondary cooling, while the energy sources in the sintering zone use the recycled off-gas heat from primary cooling and the combustion heat of off-gases from smelting, mainly CO.[20] It is assumed that the discharged off-gas temperatures from the primary and secondary cooling zones are the same as the recycled hot gas temperatures in the drying and sintering zones.
- Modelling of prereduction (Case 3) is assumed to take place in the drying (travelling grate) and prereduction (rotary kiln) zones. The energy sources, including pulverized coal and recycled off-gas from smelting, are combusted at the end of rotary kiln. The off-gas heat from the rotary kiln will be reused in the drying zone.
- The thermal energy of the in- and outgoing source in the process is calculated by using Eqs. 15–17. $\Delta H_{\text{mixture}}$ stands for the enthalpy change of the mixture. x_i represents the molar fraction of the compound i (i = Fe, Cr, Cr_2O_3, FeO, Fe_2O_3, SiO_2, MgO, CO_2, etc.). Here, an ideal mixture is assumed, which means the enthalpy of mixture is zero. ΔH_i is the enthalpy increment or the heat stored in an object by raising its temperature from T_1 to T_2. Here, T_1 is normally given a reference temperature of 298.15 K. The heat capacity (C_p) is a function of temperature and is presented in a polynomial form;[28] see Eq. 17. ΔH_{trans} is the heat of phase transformation.
- The slag formation heats of complex oxides are not considered.
- The chemical reaction heat ($\Delta H_{R,T}$) at a specified temperature is the sum of the enthalpies of the products minus the sum of the enthalpies of the reactants, described in Eq. 18 (n *is* the mole of the productants or reactants).

$$\Delta H_{\text{mixture}} = \sum x_i \Delta H_i \tag{15}$$

$$\Delta \text{H} = H_2 - H_1 = \int_{T_1}^{T_2} C_p dT + \Delta H_{\text{trans}} \tag{16}$$

$$C_p = \text{a} + \text{bT} \times 10^{-3} + \frac{c}{T^2} \times 10^5 + dT^2 \times 10^{-6} \tag{17}$$

$$\Delta H_{R,T} = \sum n_{\text{product}} H_{\text{product},T} - \sum n_{\text{reactant}} H_{\text{reactant},T} \tag{18}$$

Total Energy Consumption and Greenhouse Gas Emission of a HC FeCr Production

The total greenhouse gas emission from the ferrochrome production process can be calculated by using Eq. 19.

$$E_i = EF_i \times Q_i \tag{19}$$

where E_i stands for the GHG emission from the contribution source i (i = fuel, coke, quartzite, etc.) and Q is the amount of the contribution source, such as energy, fuel and input raw materials. Furthermore, EF_i is the emission factor (EF) of contribution source i (i = fuel, coke, quartzite, etc.). Emission factor is a conversion factor that describes the release of greenhouse gases when consuming a resource. The considered GHG emission sources in

Table I. Conversion factors of inventory

	Primary energy	Emission factor
Electricity (coal)[a]	PEF: 0.34	1 kgCO_2-eq/kWh
Electricity (natural gas)[a]	PEF: 0.4	0.5 kgCO_2-eq/kWh
Electricity (oil)[a]	PEF: 0.37	0.65 kgCO_2-eq/kWh
Electricity (hydro)[a]	PEF: 0.95	0.02 kgCO_2-eq/kWh
Electricity (wind)[a]	PEF: 0.5	0.0046 kgCO_2-eq/kWh
Electricity (solar)[a]	PEF: 0.34	0.058 kgCO_2-eq/kWh
Electricity (biomass)[a]	PEF: 0.23	0.093 kgCO_2-eq/kWh
Electricity (China)[b]	PEF=0.364	0.851 kgCO_2-eq/kWh
Electricity (South Africa)[c]	PEF=0.371	0.94 kgCO_2-eq/kWh
Electricity (Finland)[d]	PEF=0.609	0.113 kgCO_2-eq/kWh
Electricity (Kazakhstan)[c]	PEF=0.363	0.84 kgCO_2-eq/kWh
Diesel (road transport)[f]	43.3 MJ/kg	0.0752 kgCO_2-eq/MJ
Coal[f]	27.5 MJ/kg	0.0953 kgCO_2-eq/MJ
Anthracite[f]	29 MJ/kg	0.099 kgCO_2-eq/MJ
Coke[f]	28.5 MJ/kg	0.1077 kgCO_2-eq/MJ
Electrode[g]	20 MJ/kg	4.313 kgCO_2-eq/kg
Oxygen[h]	5.3 MJ/kg	0.5 kgCO_2-eq/kg
Bentonite[i]	1.5 MJ/kg	0.04 kgCO_2-eq/kg
Quartzite[j]	0.1 MJ/kg	0.01 kgCO_2-eq/kg
Limestone[k]	0.07 MJ/kg	0.45 kgCO_2-eq/kg

[a]The PEF and emission factor of electricity by different energy sources refer to Ref. 31–36, used for calculating the PEF and emission factor of the grid mix when the data are not available [b]A typical power generation in Inner Mongolia (85% coal +15% wind) is assumed to calculate PEF and emission factor[37] [c]PEF is calculated based on the power-generated energy source in 2020 (88% coal +5% nuclear +2% hydro +2% wind +2% solar)[38] The emission factor is based on year 2011[39] [d]PEF is calculated based on the power generated energy source in 2020 (34% nuclear +23% hydro +16% biomass +12% wind +8% coal +5% gas)[38] The emission factor is based on year 2016[40] [e]PEF is calculated based on the power generated energy source in 2020 (50% coal +25% gas +25% oil)[38] The emission factor is based on Ref. 41 [f]Energy and emission factor are based on Refs. 42 and 43 [g]Electrode: energy was estimated from literature data,[38] including carbonization and graphitization data. Emission is based on Ref. 44 [h]Oxygen: assume 0.5 kWh/Nm^3 electricity (coal powered) is required for generating oxygen gas [i]Bentonite: energy and emission factors are estimated based on Ref. 45 [j]Quartzite: energy factor is estimated based on 0.02 MJ/kg electricity and 0.046 MJ/kg diesel,[46] using coal-powered electricity [k]Limestone: energy and emission factor is estimated based on 0.02 MJ/kg electricity (coal powered) and 0.01 MJ /kg diesel[46]

this model are from CO_2, CH_4 and N_2O. Therefore, the emission factor is the sum of the three gas emissions. The Global Warming Potential (GWP) was calculated to allow a comparison of greenhouse effects of different gases by providing a common measurement unit, carbon dioxide equivalent (CO_2-eq). For example, GWP_{100} (CH_4) = 28 and GWP_{100} (N_2O) = 265[29] indicate that greenhouse effects from the CH_4 and N_2O gases are 28 and 265 times the effect from CO_2 gas over 100 years.

Electricity is termed as secondary energy source. The generation of electricity depends on the conversion of other forms of energy, such as the thermal energy from the fuel combustion (natural gas, coal, oil, biomass, etc.), kinetic energy from water and wind, solar energy and geothermal power, etc. The actual amount of energy generated by electricity should be converted into primary energy. Here, the primary energy factor (PEF) is typically used for such a conversion value.[30] The primary energy factor is the ratio of energy consumed in power plant (E_{plant}) and the consumed electricity by users ($E_{\text{electricity}}$); see Eq. 20.

$$PEF = E_{\text{electricity}}/E_{\text{plant}} \tag{20}$$

The PEF values of electricity can be found in Table I. In addition to the primary energy factor, the local grid mix of fuel sources for electricity is considered to generate the primary energy consumption and GHG emission per unit of electricity being consumed.

Table I presents a summary of the conversion factors of inventories, which are considered in the modelling work. In this work, energy refers to the primary energy, if something else is not specified.

RESULTS AND DISCUSSIONS

The energy consumption and GHG emissions for a HC FeCr production are affected by several factors, such as electricity sources and process technologies. To investigate the impact of these factors, four popular HC FeCr supply routes are selected as cases to be studied. The four cases are denoted as follows:

- Case 1: a submerged arc furnace (**SAF**),
- Case 2: a closed submerged arc furnace with preheating (**CSAF+PH**)
- Case 3: a closed submerged arc furnace with 60% prereduction (**CSAF+PR60%)**
- Case 4: a direct-current arc furnace (**DCAF**).

Case 1 (SAF), Case 2 (CSAF+PH) and Case 3 (CSAF+PR60%) produces charge chrome, which is an economical chromium product, while Case 4 (DCAF) processes high-grade ferrochrome (69% Cr) with a high-grade chromite (51.2% Cr_2O_3). The process flow and system boundary of the four supply cases are given in Fig. 2.

Inventory Data of HC FeCr Production

As mentioned in previous sections, the modelling follows some defined steps to calculate the inventory data. The prerequisite is the chemistry of the feedstock and some default parameter values such as the operation temperature and metal recovery rate. These data were collected from various sources such as scientific articles, textbooks and surveys. The authors have cross-compared and scrutinized data between sources and then selected the input data considered to be the most accurate for the purpose of the present modelling work. The collected data from the public domain are not fully verified, which may have their own limitations or uncertainty in results, such as out-of-data information. Such uncertainties can be reduced by implementing more detailed and recent inventory data for each process technology;[49] however, the main purpose of this study was to compare the energy consumption and GHG performance for the four common supply routes of producing HC FeCr. Thus, the results should be taken as indicative rather than definitive.

The material chemical compositions and process temperatures used in the process modelling are tabulated in supplementary Tables S-2 and Table S-3.

Table II presents the calculated inventory of 1 tonne HC FeCr through process modelling. This inventory is applied in estimating the energy consumption and GHG emissions when using the different production technologies. The mass and energy balances for all four cases are shown in supplementary Table S-4, Table S-5, Table S-6 and Table S-7. The estimated site-specific inventory data were then compared with the reported plant values. Table III shows an example of Case 2 (CSAF+PH), for which extensively reported plant data are available.[3] The relative error of modelled material/electricity consumption and plant data is $< 6\%$, indicating good agreement between predictions and plant data.

Energy Consumption and GHG Emission of HC FeCr Production

The total energy consumption and GHG emission from the process modelling of four cases in producing HC FeCr alloys are shown in Fig. 3. The required energies for manufacturing HC FeCr in Case 1 (SAF), Case 2 (CSAF+PH), Case 3 (CSAF+PR60%) and Case 4 (DCAF) are 59 GJ/t FeCr, 40 GJ/t FeCr, 49 GJ/t FeCr and 59 GJ/t FeCr, respectively. As suggested from Fig. 3a-1, smelting is the most energy-intensive stage; specifically, it accounts for 64%-98% for the four studied cases. Most of the energy is consumed for electricity generation in smelting (Fig. 3a-2) for Case 1-SAF (74%), Case 2-CSAF+PH (52%) and Case 4-DCAF (76%). Regarding Case 3 (CSAF+PR60%), the low electricity contribution (48%) is offset by the prereduction from coal before smelting. The electricity use may vary in the prereduction degree before smelting. In terms of carbon footprint, the GHG emissions are estimated as 5.5 tCO_2-eq/t FeCr (Case 1 SAF), 1.8 tCO_2-eq/t FeCr (Case 2 CSAF+PH), 4.8 tCO_2-eq/t FeCr (Case 3 CSAF+PR60%), and 5.3 tCO_2-eq/t FeCr (Case 4 DCAF), respectively. Among those, the main emissions come from the smelting stage (69–99%), as seen in Fig. 3b-1. Furthermore, the emission contribution from electricity varies between 20% to 71%.

The relatively simple operations, Case 1(SAF) and Case 4 (DCAF) route, indicate a high energy demand and high GHG emissions. Case 1 (SAF) has a low metal yield (75%) and the low energy off-gas is difficult to recycle because of the leakage of air from the unsealed furnace. For Case 4 (DCAF), the metal yield is the highest (90%), but the heat loss is the highest among cases (28%).

Compared with Case 1 (SAF) and Case 4 (DCAF), Case 2 (CSAF+PH) shows a decrease in energy use (around 31%) and carbon emissions (66%). One of the reasons is the combustion of furnace gas from other process steps (e.g., sintering, preheating), which generates approximately 6 GJ/t FeCr. The utilization of secondary energy brings a reduction of 16% of the total energy use, which can not only lower the energy costs but also lower the carbon emissions during FeCr production. Moreover, Case 2 (CSAF+PH) results in the lowest GHG emissions among cases because of the electricity source (mainly nuclear and hydropower).

Case 3 (CSAF+PR60%) includes 4 GJ/t FeCr off-gas powered combustion in prereduction, but the total energy reduction ratio is only 8%. This is due to the increased use of reductant in the prereduction step. It is necessarily noted that Case 3 (CSAF+PR60%) has a high initial capital cost but low capital cost per tonne.[23] The economic competitiveness of process technology CSAF+PR60% is offset by its heavy pollution causing a larger greenhouse gas effect.

In the four studied cases, the contained chromium content varies between 52% to 69%. This makes it difficult for a downstream consumer, for instance, a stainless steel manufacturer, to directly evaluate the upstream carbon footprint or scope 3 value when using HC FeCr from different suppliers. As shown in Fig. 2, Case 1(SAF), Case 2 (CSAF+PH) and Case 3 (CSAF+PR60%) produce HC FeCr. which has a relatively lower Cr % in the alloy (52–55%Cr) compared to that of HC FeCr in Case 4-DCAF (69%Cr). Figure 4 suggests that the energy

Case	Mine	Ore (Cr_2O_3%)	Smelter	Process	FeCr Alloy (Cr%)
1	South Africa	Chromite (40.2)	China	SAF	Charge chrome (53%)
2	Finland	Chromite (45.69/35.68)	Finland	CSAF+PH	Charge chrome (55%)
3	South Africa	Chromite (40.2)	South Africa	CSAF+PR60%	Charge chrome (52%)
4	Kazakhstan	Chromite (51.2)	Kazakhstan	DCAF	Ferrochrome (69%)

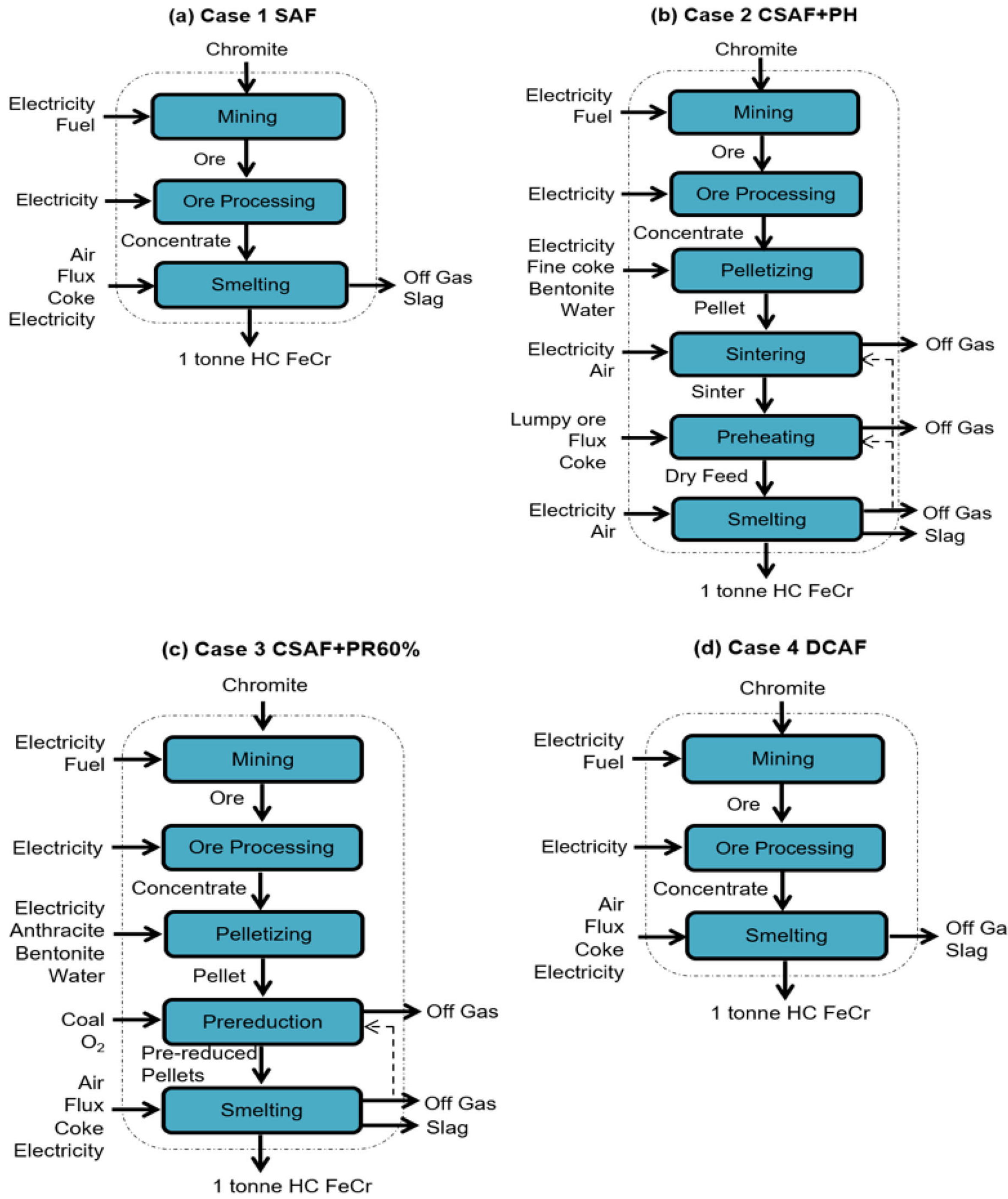

Fig. 2. Process flows and system boundaries of four HC FeCr products: (a) Case 1 SAF, (b) Case 2 CSAF + PH, (c) Case 3 CSAF + PR60% and (d) Case 4 DCAF.[2,3,47,48]

Table II. Calculated inventory and output through process modelling of 1 tonne of HC FeCr production

Inventory	Unit	Case 1 SAF	Case 2 CSAF+PH	Case 3 CSAF+PR60%	Case 4 DCAF
Mining +ore processing					
Ore[a]	t	2604	2265	2155	2225
Diesel[b]	kg	4.4	3.9	3.7	3.8
Electricity (mining)[b]	kWh	65	57	54	107
Electricity (beneficiation)[b]	kWh	52	45	43	45
Pelletizing					
Electricity[c]	kWh	–	2.3	2.2	–
Bentonite[c]	kg	–	15	43	–
Fossil carbon[c]	kg	–	Fine coke: 7.5	Anthracite: 292	–
Water[c]	kg	–	161	255	–
Sintering[d]*/prereduction*[e]					
Electricity[f]	kWh	–	94	–	–
Recycled gas[g]	MJ	–	3386	3925	–
Pulverized coal[g]	kg		–	164	
Air	Nm^3	–	4324	16	–
Oxygen[h]	Nm^3		–	378	
Smelting					
Fuel (preheating, off-gas)[i]	MJ	–	2930	–	–
Air (preheating)	kg	–	711	–	–
Air (smelting)[j]	kg	300	20	20	20
Electricity[k]	kWh	4297	3102	2336	4364
Coke[l]	kg	511	441	294	475
Electrode[m]	kg	22	9	20	15
Quartzite[n]	kg	105	299	206	93
Limestone[n]	kg	145	0	300	0
Alloy	t	1	1	1	1
Cr	%	53	55	52	69
C	%	6.1	6.3	6.7	8
Si	%	2.5	3.9	3.9	0.13
Slag	t	1.47	1.17	1.3	1.1
Cr recovery[o]	%	75	84	88	88

[a] In Case 2, the ore charging is 36% lumpy ore+64% pellet[3] [b] Diesel and electricity consumption refers to Refs. 50 and 51 [c] The bentonite weight in pelletizing of Case 2 and Case 3 is assumed as 1% and 2%, respectively.[52] The fossil carbon mass in Case 2 is calculated assuming a 0.45% C content in pellets,[53] while the anthracite content in Case 3 is based on the pre-reduction ratio. It is assumed that the moisture after pelletizing is 10% and that the pelletizing energy is 1 kWh/tonne ore [d] Only oxidation of FeO occurs during sintering, and the Fe^{2+}/Fe_{tot} ratio in the sintered pellet is 0.3[48] [e] It is assumed that 80% of the carbon in the green pellet is used for a partial reduction while the rest reacts with the CO_2 gas [f] The electricity consumption of steel belt is assumed to have a value of 65 kWh/tonne sinter[54] [g] The supplied energy in Case 3 sintering is 50% from coal-powered combustion +50% off-gas-powered combustion. It is assumed that the reaction for off-gas combustion is only considering oxidation with CO [h] The coal and off-gas are combusted with pure oxygen gas at the end of rotary kiln[23] [i] Assuming that all the free water in coke, quartzite, ores together with 50% bond water in ores are removed [j] Assuming 20 kg air leakage in closed furnace in Cases 2–4, which forms CO_2. In Case 1, it is assumed that 300 kg air flows into semi-open SAF in which 50 kg air forms CO_2 while the rest goes to the off-gas [k] The powers on heat losses in the electric furnace are 18%, 15%, 15% and 28% for Case 1, Case 2, Case 3 and Case 4, respectively[3,24] [l] All the Cr_2O_3 is reacted with C to form two carbides, Cr_7C_3 and Cr_3C_2. The percentages of Cr_2O in smelting in forming Cr_7O_3 and Cr_3C_2 are about 70% and 30%, respectively, for all cases. Besides, it is assumed that 90% of the incoming H_2O reacts with C while the rest is vaporized as steam in off-gas. The ratio of generated CO_2 reacting with C is considered 60%, while the rest is emitted in the off-gas [m] The electrode consumption is based on Ref. 6 [n] The basicities $(CaO+MgO)/SiO_2$ are 1.4, 0.81, 1.1 and 1.55 for Case 1, Case 2, Case 3 and Case 4, respectively[3,55] [o] The metal recovery refers to Ref. 2, 3, and 47

consumptions and GHG emissions for producing 1 tonne of Cr in the process of SAF, CSAF+PH, CSAF+PR60% and DCAF are 74 −111 GJ and 3.3 −10.3tCO_2-eq, respectively.

Table IV shows a comparison of the different assessment studies for HC FeCr productions with the CSAF+PH and CSAF+PR60% processes. The modelled GHG emissions for the production route of Case 2 (CSAF+PH) and Case 3 (CSAF+PR60%) in this work are 14–30% lower compared to other studies.[51,56,57] There are a few reasons that could explain this. First, in this work, coke in Case 2 CSAF+PH route has a carbon content of 78% and the applied carbon emission factor of coke is 0.1077 kgCO_2-eq/MJ independent of the composition. Material consumption in current process modelling is highly dependent on the material composition. In others' work,[51,56,57] the reductant with low carbon content may be used but not mentioned. Thus, it contributes to a higher reductant demand. Second,

Table III. Comparison of modelling results with plant data for Case 2 (CSAF+PH)[3]

	Plant data	Modelling result	Relative error %[a]
Electricity	3070 kWh/t alloy	3102 kWh/t alloy	1.0%
Pellet	1460 kg/t alloy	1450 kg/t alloy	– 0.7%
Lumpy ore	821 kg/t alloy	815 kg/t alloy	– 0.7%
Coke	470 kg/t alloy	441 kg/t alloy	– 6%
Quartzite	301 kg/t alloy	299 kg/t alloy	– 0.7%
Alloy	34.86%Fe, 53.61%Cr, 3.91%Si,7.1%C	35.2% Fe, 54.6%Cr, 3.9%Si, 6.3%C	–
Slag	3.83%Fe, 8.81%Cr, 31.33%SiO_2, 23.66%MgO, 1.58%CaO, 24.92%Al_2O_3, 0.72%C	3.71%Fe, 8.87%Cr, 30.4%SiO_2, 23.97%MgO, 1.37%CaO, 26.5%Al_2O_3, 0%C	–
Off-gas volume	688 Nm^3/t alloy 84.82%CO,6.01%CO, 5.96% H_2, 0.4% H_2O,2.81%N_2	653 Nm^3/t alloy 91%CO, 2.6%CO_2, 4%H_2, 0.45% H_2O, 1.88%N_2	– –
Basicity	0.8	0.81	–
Slag/alloy	1.21	1.17	–

[a]Relative error (%) = (modelling result-plant data)/plant data*100

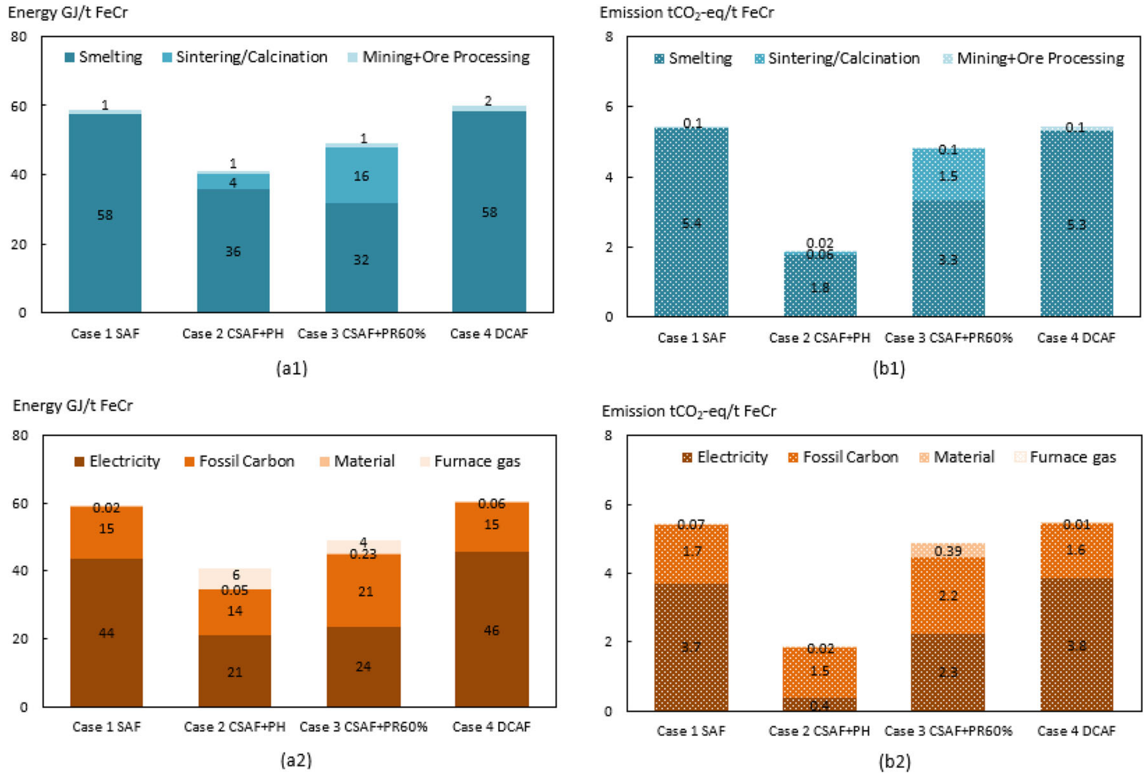

Fig. 3. (a1) Energy consumption (GJ/t FeCr) and (b1) GHG emissions (tCO_2-eq/t FeCr) of HC FeCr production along from sub-process. (a2) Energy consumption (GJ/t FeCr) and (b2) GHG emissions (tCO_2-eq/t FeCr) of HC FeCr production along with the contribution source

the CSAF+PH process route uses a Finnish grid mix (34% nuclear+23% hydro) in the current work and this is probably lower than the electricity emission factor of Australia. Furthermore, the variance may come from the difference in the applied carbon emission factors for electricity. Taking the process of CSAF+PH as an example, a 0.113 kgCO_2-eq/kWh value is used as the Finnish electricity emission factor in this work. The data were collected from public data in 2020, while in Hamuyuni et.al's work[56,57] the Finnish grid mix emission factor (0.23882 kgCO_2-eq/kWh) was collected from the commercial database Ecoinvent version 3.5 (2018). The low electricity emission factors in this work

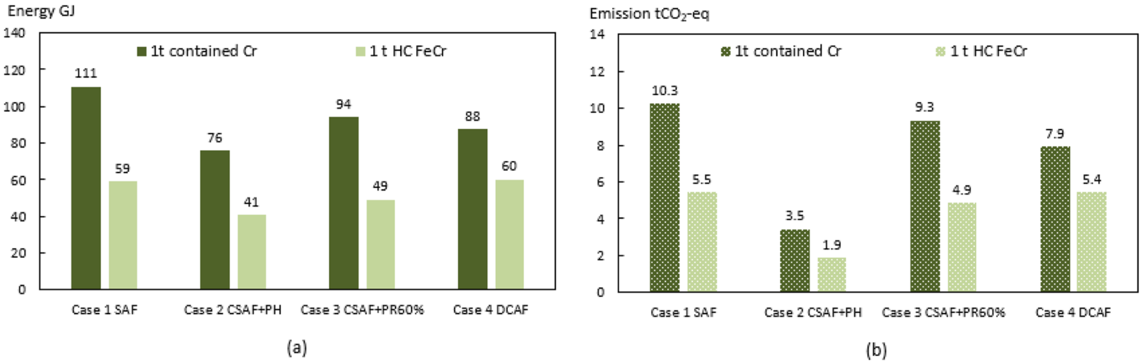

Fig. 4. (a) Energy consumption (GJ) and (b) GHG emissions (tCO_2-eq) based on 1 tonne HC FeCr and 1 tonne contained Cr

Table IV. Comparisons of assessment of 1 tonne HC FeCr production in energy consumption and GHG emission

	Ore (Cr_2O_3%)	FeCr (Cr%)	Location	Electricity		Reductant kg	Energy GJ	GHG scope (tCO_2-eq)			
				kWh	Source			1	2	3	Total
CSAF+PH											
IPCC[58]		58–60	Norway			440	–	1.6	–	–	–
Haque et al.[51]	25.5	53	Australia	4528	Main hydro	630	77	–	–	–	3.04
	25.5	53	Australia	4528	Main coal	630	–	–	–	–	7.22
Hamuyuni et al.[56,57]	40.6	49	Finland	3540	–	510	–	–	–	0.92	2.295
This work	45.69/35.68	55	Finland	3102	34% Nuclear + 23% Hydro	441	40	1.4	0.4	0.02	1.82
CSAF+PR60%											
Hamuyuni et al. (2021)[56,57]	40.6	49	SA	2600	–	820 + 60	–	–	–	1.04	5.612
This work	40.2	52	SA	2336	88% Coal	292 + 294	48	2.2	2.2	0.4	4.8

may be due to the sustainable technology upgrading of the power plants in recent years.

Effect of Electricity on the Energy Use and GHG Emission of HC FeCr Production

"Energy Consumption and GHG Emission of HC FeCr Production" Section shows that the production of HC FeCr is an electricity-intensive process. Here, based on the inventory from the four cases, scenarios when using different electricity sources, coal-powered and hydro-powered electricity, are compared and discussed. The use of a coal-powered electricity scenario in Fig. 5 suggests that the FeCr alloy with coal-based electricity has a typical carbon footprint value between 4.7 and 6.1 tCO_2-eq/t FeCr depending on the supply routes. The relatively simple operation processes, such as Case 1 (SAF) and Case 4 (DCAF), have the advantages of having low investment costs, low raw material costs and being easy to operate; however, these are high carbon burden processes. With the strict environmental regulations and the implementation of a carbon border adjustment mechanism, these production technologies will become less attractive in the future.

Compared to the conventional SAF route (Case 1), the utilization of the furnace off-gas in Case 2 CSAF+PH will reduce the carbon footprint of 1 tonne coal-powered FeCr by 23%. The CO_2 mitigation when upgrading Case 1 (SAF) to Case 3 (CASAF+PR60%) is relatively low, only emitting 18% less GHG emissions. Moreover, the use of sustainable electricity powered by hydro-energy results in a further reduction of the GHG emission. For the advanced closed furnace technology, Case 2 (CSAF+PH) and Case 3 (CSAF+PR 60%), the GHG emissions are decreased by 68% and 47%, respectively.

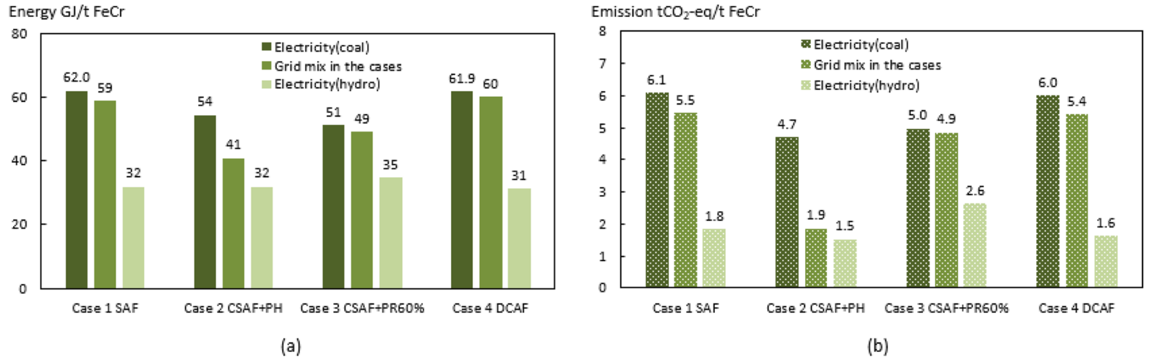

Fig. 5. (a) Energy consumption (GJ/t FeCr) and (b) GHG emissions (tCO_2-eq/t FeCr) of HC FeCr production with different electricity scenarios: coal-powered, grid mix in the cases and hydro-powered

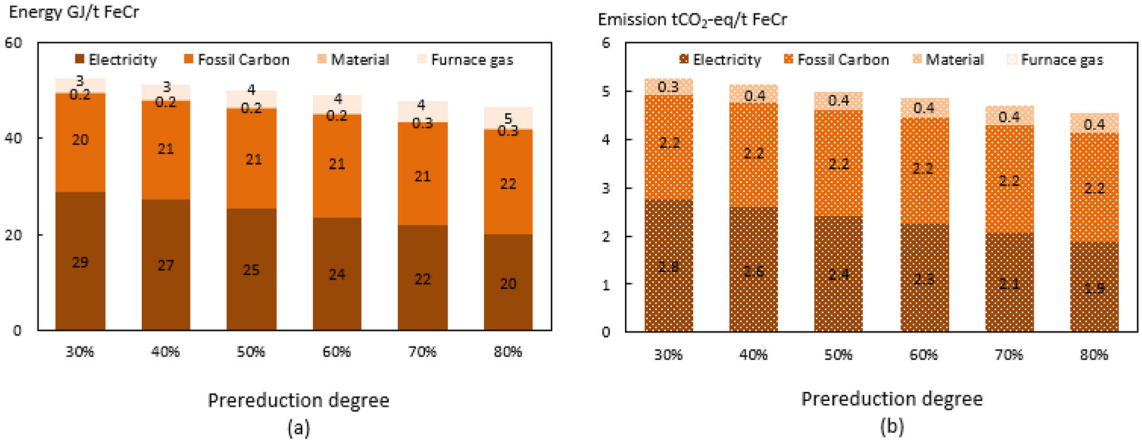

Fig. 6. (a) Energy consumption (GJ/t FeCr) and (b) GHG emissions (tCO_2-eq/t FeCr) of HC FeCr production with different prereduction degrees (based on inventory of Case 3 CSAF+PR60%)

Effect of Prereduction Degree on the Energy Use and GHG Emission of HC FeCr Production

Compared to the conventional SAF process (Case 1), the CSAF+PR process (Case 3) not only recycles furnace gas as a secondary energy but also pre-reduces the ore before the smelting step. This significantly reduces the electricity requirement (from 4297 kWh/t FeCr to 2336 kWh/t FeCr) and coke (from 511 kg/t FeCr to 294 kg/t FeCr) during smelting, as suggested in Table II. However, these reductions are offset by the increased use of reductants in the pre-reduction step. Therefore, a parameter study in terms of the effect of the prereduction degree on the total GHG emissions of FeCr production was performed. As shown in Fig. 6, an increase of prereduction degree from 30% to 80% results in a 31% reduction in electricity-related primary energy, while the fossil carbon-related energy is increased by 7%. The total energy is decreased by 11%, while the reduction ratio of the total GHG emissions is 14%. Notably, the high prereduction degree in the rotary kiln decreases the productivity and pellet output. Meanwhile, the risk of carbon burn-off and oxidation of the pellets increased. To keep an optimum net energy output in a rotary kiln, the pre-reduction degree should be monitored and controlled at a proper level.[23]

Effect of Hot Charge Temperature on the Energy Use and GHG Emission of HC FeCr Production

Other than the prereduction degree, pellets hot discharged from the rotary kiln have some considerable enthalpy (1400 °C) that could be utilized to improve the energy effectiveness during the production. Figure 7 shows the changes of energy requirement and carbon footprint of FeCr production for Case 3 CSAF+PR60% when hot charging the pellets between 100 °C to 1000 °C. The energy saving and decarbonizing potential when raising the hot charge temperature from 100 °C to 1000 °C are both approximately 10%.

CONCLUSION

In the current work, the energy consumption and GHG emissions when producing 1 tonne of HC FeCr from cradle to gate have been evaluated in four cases, representing the following current four

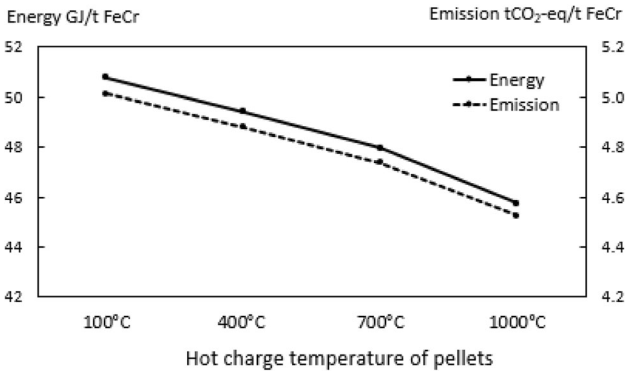

Fig. 7. Energy consumption (GJ/t FeCr) and GHG emissions (tCO_2-eq/t FeCr) of HC FeCr production with different hot charge temperatures for pellets (based on inventory of Case 3 CSAF+PR60%)

existing supply routes of HC FeCr: (1) a submerged arc furnace (SAF), (2) a closed submerged arc furnace with preheating (CSAF+PH), (3) a closed submerged arc furnace with 60% prereduction (CSAF+PR60%) and (4) a DC arc furnace (DCAF). The modelled inventory data are further used in parameter studies to explore the potential environmental improvements in producing HC FeCr, using the developed process model based on mass and energy conservations. The conclusion can be summarized as follows:

- The estimated energy requirement for producing HC FeCr varies between 40 and 59 GJ/t FeCr (74-111 GJ/t Cr), while the associated GHG emissions vary between 1.8 and 5.5 tCO_2-eq/t FeCr (3.3-10.3 tCO_2-eq/t Cr) depending on the supply route. Among these, smelting is the most energy and emission-intensive stage, which accounts for 64–98% of the total energy use and 69–99% of the total GHG emissions. Specifically, as the main energy source of the smelting furnace, the electricity plays a vital role in determining the environmental impact of a produced FeCr alloy.
- The GHG emissions for 1 tonne HC FeCr produced using coal-powered electricity is between 4.7-6.1 tCO_2-eq/t FeCr. Relatively simple operations, such as Case 1 (SAF) and Case 4 (DCAF), have high energy demands and high carbon emissions due to low metal yields and high thermal losses, respectively. The upgrading of Case 1 (SAF) to a closed furnace Case 2 (CSAF+PH) and Case 3 (CSAF+PR60%) will result in an emission reduction of 23% and 18%, respectively. Moreover, the use of a sustainable hydro-powered electricity results in a further decrease of 68% and 47% in the total GHG emission for Case 2 and Case 3, respectively.
- Regarding Case 3 (CSAF+PR60%), when the prereduction degree is increased from 30% to 80%, the reduced electricity-related primary energy in smelting is 31%. This is offset by a 7% increment of a fossil carbon-related energy. The total GHG emissions are reduced by 14% when increasing the prereduction degree from 30% to 80%; however, the prereduction degree should be kept at a proper level to reach an optimum net enthalpy in the pellet output in a rotary kiln. In addition, the energy saving and decarbonizing potential when the charge temperature of hot feed from 100 °C to 1000 °C are both 10%.

The study indicates that the proposed process model is feasible for generating site-specific inventory data and allowing for parameter studies as well as supporting companies to improve the transparency of the environmental performance in the FeCr value chain.

SUPPLEMENTARY INFORMATION

The online version contains supplementary material available at https://doi.org/10.1007/s11837-023-05707-8.

ACKNOWLEDGEMENTS

This study was funded by the research scholarship received from Bergshögskolans jubileumsfond VT-2021-0040. We appreciate the research support from Kobolde & Partners AB and Anders Tilliander for the discussions during this study.

FUNDING

Open access funding provided by Royal Institute of Technology.

CONFLICT OF INTEREST

The authors declare that they have no conflict of interest.

OPEN ACCESS

REFERENCES

1. Y. Yu, S. Shironita, K. Souma, and M. Umeda, *Heliyon* 4, e00958 https://doi.org/10.1016/j.heliyon.2018.e00958 (2018).
2. I. Geldenhuys, Aspects of DC chromite smelting at Mintek–an overview. in Paper presented at the 13th International Ferro-Alloys Congress (INFACON XIII), Kazakhstan, Almaty, 9–12 (2013).
3. J. Basson and J. Daavittila, *Handbook of Ferroalloys*, ed. M. Gasik (Butterworth-Heinemann, Oxford, 2013), pp 317–363.
4. ISSF, Stainless Steel and CO2 : Facts and Scientific Observations (ISSF, 2015), https://aceroplatea.es/docs/ISSF_Stainless_Steel_and_CO2.pdf. Accessed 29 August 2022.
5. GHG Protocol"Corporate Value Chain (Scope 3) Accounting and Reporting Standard" (GHG Protocol, 2011), https://ghgprotocol.org/sites/default/files/standards/Corporate-Value-Chain-Accounting-Reporing-Standard-EReader_041613_0.pdf. Accessed 2022-12-27.
6. USGS, Chromium life cycle study (U.S. Department of the Interior, Bureau of Mines 1995), https://hero.epa.gov/hero/index.cfm/reference/details/reference_id/3840037. Accessed 29 August 2022.
7. M. Ripa, G. Fiorentino, V. Vacca, and S. Ulgiati, *J. Cleaner Prod.* 142, 445–460 https://doi.org/10.1016/j.jclepro.2016.09.149 (2017).
8. B. Poujol, A. Prieur-Vernat, J. Dubranna, R. Besseau, I. Blanc, and P. Pérez-López, *J. Ind. Ecol.* 24, 248–262 https://doi.org/10.1111/jiec.12989 (2020).
9. P. Lundqvist, Mass and Energy Balances over the Lime Kiln in a Kraft Pulp Mill, Master's Thesis, Uppsala University (2009).
10. M. Kirschen, V. Risonarta, and H. Pfeifer, *Energy* 34, 1065–1072 https://doi.org/10.1016/j.energy.2009.04.015 (2009).
11. P. Liu, B. Li, S.C.P. Cheung, and W. Wu, *Appl. Therm. Eng.* 109, 542–559 https://doi.org/10.1016/j.applthermaleng.2016.08.095 (2016).
12. W. Wei, P.B. Samuelsson, A. Tilliander, R. Gyllenram, and P.G. Jönsson, *Energies* 13, 5664 (2020).
13. N.E. Kamfjord, Mass and energy balance of the silicon process: improved emission standards, Ph.D Thesis, Norwegian University of Science and Technology, Trondhelm, Norway (2002).
14. USGS, "Minerals Yearbook Chromium 2020" (USGS, 2022), https://www.usgs.gov/centers/national-minerals-information-center/chromium-statistics-and-information. Accessed 29 August 2022.
15. M.I. Gasik, *Handbook of Ferroalloys*, ed. M. Gasik (Butterworth-Heinemann, Oxford, 2013), pp 267–316.
16. S. Agarwal, J. Pal, and D. Ghosh, *Ironmak. Steelmak.* 43, 97–111 https://doi.org/10.1179/1743281215Y.0000000054 (2016).
17. G. Kapure, C. Kari, S. Mohan Rao and K.S. Raju, Use of chemical energy in submerged arc furnace to produce ferrochrome: prospects and limitations. Paper presented at the 11th International Ferro-Alloys Congress (INFACON XI), Cape Town, South Africa, 2007.
18. Roskill, China closing small ferrochrome furnaces (Roskill, 2021), https://www.globenewswire.com/news-release/2021/01/28/2165637/0/en/Roskill-China-closing-small-ferrochrome-furnaces.html#:~:text=The%20closure%20of%20small%20and,the%20development%20of%20new%20capacity. Accessed 29 August 2022.
19. J.P. Beukes, N.F. Dawson, P.G.V. Zyl, and J.S. Afr, *J. S. Afr. Inst. Min. Metall.* 110, 743–750 (2010).
20. H. Krogerus, J. Daavittila, J. Vehvilainen, and M. Honkaniemi, The application of steel belt technology for the sintering of manganese ore fines. in Paper presented at the 8th International Ferro-Alloys Congress (INFACON XIII), Beijing, China, (2013).
21. J. Keihäs, P. Mäkelä, J. Ollila, and L. Hekkala, CFD modelling of the steel belt sintering process. in Paper presented at the 11th International Ferro-Alloys Congress (INFACON XI), New Delhi, India, 18–21 (2007).
22. P. Niemelä, H. Krogerus, and P. Oikarinen, Formation, characteristics and utilisation of CO-gas formed in ferrochromium smelting. in Paper presented at the 10th International Ferroalloys Congress (INFACON X), Cape Town, South Africa 1–4 (2004).
23. O. Naiker, The development and advantages of XSTRATA's Premus process Paper presented at the International Ferro-Alloys Congress (INFACON XI), New Delhi, India, 18-21 (2007).
24. K. Bergman and B. Kjellberg, DC arc furnace technology applied to smelting applicaiton. in Paper presented at the 9th International Ferroalloys Congress (INFACON IX), Quebec, Canada, 3–6 (2001).
25. I. Mc Dougall, *Handbook of Ferroalloys*, ed. M. Gasik (Butterworth-Heinemann, Oxford, 2013), pp 83–138.
26. C.C. Ugwuegbu, *Innov. Syst. Design Eng.* 3, 48–54 (2012).
27. J. Daavittila, M. Honkaniemi, and P. Jokinen, *J. S. Afr. Inst. Min. Metall.* 104 (2004).
28. I. Barin, and O. Knacke, *Thermochemical Properties of Inorganic Substances* (Springer, Berlin, Heidelberg, Berlin, 1973).
29. IPCC, Climate Change 2013: the physical science basis. Contribution of Working Group I to the Fifth Assessment Report of the Intergovernmental Panel on Climate Change (IPCC, 2013), https://www.ipcc.ch/report/ar5/wg1/. Accessed 29 August 2022.
30. M. Dixit, C. Culp, and J. Fernandez-Solis, *RSC Adv.* https://doi.org/10.1039/C4RA08989H (2014).
31. IEA, Energy Efficiency Indicators for Public Electricity Production from Fossil Fuels" (IEA, 2008), https://www.iea.org/reports/energy-efficiency-indicators-for-public-electricity-production-from-fossil-fuels. Accessed 29 August 2022.
32. UK_Parliament, Carbon footprint of electricity generation (postnote) (UK_Parliament, 2006), https://www.parliament.uk/documents/post/postpn268.pdf. Accessed 29 August 2022.
33. B.J. Lewis, J.M. Cimbala, and A.M. Wouden, *IOP Conf. Series: Earth Environ. Sci.* 22, 012020 https://doi.org/10.1088/1755-1315/22/1/012020 (2014).
34. DOE, Wind Vision: A New Era for Wind Power in the United States (DOE, 2015), https://www.energy.gov/sites/prod/files/2013/11/f4/55296.pdf. Accessed 29 August 2022.
35. DOE, Renewable electricity generation (DOE, 2012), https://www.energy.gov/sites/prod/files/2013/11/f4/55296.pdf. Accessed 29 August 2022.
36. Biomass_Energy_Resource_Center, Biomass energy: efficiency, Scale, and Sustainability (2009), https://www.biomasscenter.org/policy-statements/FSE-Policy.pdf Accessed 29 August 2022 Biomass Energy Resource Center.
37. Huaon, Statistical analysis of power generation and structure in Inner Mongolia Autonomous Region from 2015 to 2021(in Chinese) (Statistical analysis 2022), https://m.huaon.com/detail/782053.html. Accessed 29 August 2022.
38. IEA, Electricity generation by source (IEA, 2020), https://www.iea.org/data-and-statistics/charts/electricity-generation-by-source-oecd-2000-2020. Accessed 29 August 2022.
39. National_Business_Initiative, South Africa's Grid Emission Factor (National_Business_Initiative 2013), https://www.nbi.org.za/wp-content/uploads/2016/08/South-Africas-Grid-Emission-Factor-Mar-13.pdf.
40. EEA, Greenhouse gas emission intensity of electricity generation by country (EEA, 2021), https://www.eea.europa.eu/data-and-maps/daviz/co2-emission-intensity-10/#tab-chart_2. Accessed 29 August 2022.
41. GCF, GCF-EBRD Kazakhstan Renewables Framework (Green Climate Fund, 2017), https://www.greenclimate.fund/document/gcf-ebrd-kazakhstan-renewables-framework. Accessed 29 August 2022.

42. IPCC, 2006 IPCC Guidelines for National Greenhouse Gas Inventories (2006), https://www.ipcc-nggip.iges.or.jp/public/2006gl/. Accessed 29 August 2022.
43. IPCC, Good Practice Guidance and Uncertainty Management in National Greenhouse Gas Inventories (2001), https://www.ipcc-nggip.iges.or.jp/public/gp/english/ Accessed 29 August 2022.
44. Worldsteel, CO2 Data Collection-User Guide, version 10 (Worldsteel, 2021), https://worldsteel.org/wp-content/uploads/CO2-data-collection-user-guide-version-10.pdf. Accessed 29 August 2022.
45. C. Athanassopoulos and R.J. Vamos, Carbon footprint comparison of GCLs and Compacted clay liners (CETCO, 2011), https://www.cetco.com.au/DesktopModules/Bring2mind/DMX/Download.aspx?EntryId=8167&Command=Core_Download&language=en-US&PortalId=31&TabId=3140. Accessed 29 August 2022.
46. USGS, Mining Industry Energy Bandwidth Study (USGS, 2007), https://www.osti.gov/servlets/purl/1218653. Accessed 29 August 2022.
47. O. Naiker and T. Riley, Xstrata alloys in profile. in Paper presented at the Southern African Pyrometallurgy Johannesburg, 5–8 (2006).
48. T. Lintumaa, H.J. Krogerus, and P. Jokinen, Factors affecting the reducibility of sintered chromite pellets and chromite lumpy ore. Paper presented at the 11th International Ferro-Alloys Congress (INFACON XI), New Delhi, India, (2007).
49. M.J. Eckelman, *Resour. Conserv. Recycl.* 54, 256–266 https://doi.org/10.1016/j.resconrec.2009.08.008 (2010).
50. D.I. Bleiwas, Estimates of electricity requirements for the recovery of mineral commodities, with examples applied to sub-Saharan Africa (USGS, 2011), http://pubs.er.usgs.gov/publication/ofr20111253. Accessed 29 August 2022.
51. N. Haque, and T. Norgate, *J. Cleaner Prod.* 39, 220–230 https://doi.org/10.1016/j.jclepro.2012.08.010 (2013).
52. D.M.E. Bentonite, Pyrophyllite and talc in the Republic of South Africa (Department of Minerals and Energy, Republic of South Africa, 2004), https://www.dmr.gov.za/LinkClick.aspx?fileticket=FTRfs9JWbU8%3D&portalid=0. Accessed 29 August 2022.
53. H. Krogerus, T. Lintumaa, and P. Jokinen, Laboratory Investigations of the Electrical Resistivity of Cokes and Smelting Charge for Optimizing Operation in Large Ferrochrome Furnaces. in Paper presented at the Southern African Pyrometallurgy 2006 International Conference, Cradle of Humankind, South Africa 5–8 (2006).
54. Outotec, ”Steel Belt Sintering“ (Outotec, 2022), https://www.mogroup.com/portfolio/steel-belt-sintering-plant/. Accessed 29 August 2022.
55. P. Niemelä and M. Kauppi, Production, characteristics and use of ferrochromium slags. in Paper presented at the 11th International Ferro-alloys Congress (INFACON XI), New Delhi, India, 18–21 (2007).
56. J. Hamuyuni, H. Johto, A. Bunjaku, S. Vatanen, T. Pajula, P. Mäkelä, and M. Lindgren, *J. Clean. Prod.* 295, 126503 https://doi.org/10.1016/j.jclepro.2021.126503 (2021).
57. J. Hamuyuni, H. Johto, T. Haimi, A. Bunjaku, P. Mäkelä, L. Närhi, and M. Lindgren, Evaluating the carbon footprint of ferrochrome production technologies using HSC-SIM and OpenLCA software packages. in Paper presented at the 16th InInternational Ferro-Alloys Congress (INFACON XVI), (Virtual), 27–29 (2021).
58. B. Monsen, S. Olsen, and T. Lindstad, CO2-emissions from the production of manganese and chromium alloys in Norway. in Paper presented at the 56th Electric Furnace Conference, New Orleans, USA, (1998).